

Article

Micro-Doppler Estimation and Analysis of Slow Moving Objects in Forward Scattering Radar System

Raja Syamsul Azmir Raja Abdullah ^{1,*}, Ali Alnaeb ¹, Asem Ahmad Salah ¹,
Nur Emileen Abdul Rashid ², Aduwati Sali ¹ and Idnin Pasya ²

¹ Wireless and Photonic Networks Research Centre, Faculty of Engineering, Universiti Putra Malaysia (UPM), 43400 Serdang Selangor, Malaysia; gs46128@student.upm.edu.my (A.A.); asem_a@upm.edu.my (A.A.S.); aduwati@upm.edu.my (A.S.)

² Faculty of Electrical Engineering, Universiti Teknologi MARA (UiTM), 40450 Shah Alam, Selangor, Malaysia; emileen98@salam.uitm.edu.my (N.E.A.R.); idnin@salam.uitm.edu.my (I.P.)

* Correspondence: r_syamsul@upm.edu.my; Tel.: +60-3-8946-4370

Academic Editors: Francesco Soldovieri, Raffaele Persico, Xiaofeng Li and Prasad S. Thenkabail

Received: 27 April 2017; Accepted: 5 July 2017; Published: 6 July 2017

Abstract: Micro-Doppler signature can convey information of detected targets and has been used for target recognition in many Radar systems. Nevertheless, micro-Doppler for the specific Forward Scattering Radar (FSR) system has yet to be analyzed and investigated in detail; consequently, information carried by the micro-Doppler in FSR is not fully understood. This paper demonstrates the feasibility and effectiveness of FSR in detecting and extracting micro-Doppler signature generated from a target's micro-motions. Comprehensive theoretical analyses and simulation results followed by experimental investigations into the feasibility of using the FSR for detecting micro-Doppler signatures are presented in this paper. The obtained results verified that the FSR system is capable of detecting micro-Doppler signature of a swinging pendulum placed on a moving trolley and discriminating different swinging speeds. Furthermore, human movement and micro-Doppler from hand motions can be detected and monitored by using the FSR system which resembles a potential application for human gait monitoring and classification.

Keywords: micro Doppler signature; forward scatter radar; swinging pendulum; human gait

1. Introduction

Forward Scatter Radar (FSR) is a subclass of Bistatic Radar and it is being actively studied as it has many advantages such as, enhanced Radar Cross Section (RCS) at FS region and possibility of using Continuous Wave (CW) as transmitted signal which enable low radiation power requirement. Moreover, a FSR receiver circuit is reasonably simple in design, where it can detect stealth targets such as the FS RCS is practically independent from its shape and absorbs material coating [1]. Recently, the use of FSR systems has gained the interest of radar enthusiasts. As a result, FSR system has been employed in many applications (mostly no micro motion of target) such as vehicle recognition and classification [2–5], maritime target parameter evaluation [4,6], vehicles speed estimation [7], virtual microwave fences [8], and air target (airplane) detection [9]. However, the FSR's effectiveness and capability for micro-Doppler detections are still unclear, thus the study remains a broad area of research and poses fresh challenges.

When different parts of moving targets exhibit a micro-motion with respect to its global reflection center, such as vibrations or rotating movements, it produces additional frequency modulation of the reflected wave, and the generated frequency sidebands are known as micro-Doppler effects [10]. The micro-Doppler extractions from both of the monostatic and bistatic radar provide some exciting results [10,11]. The micro-Doppler effect is used in many applications such as for specific types

of vehicle identification, and determining the speed of their engines and their movement [12,13]. The micro-Doppler signal extraction for different forms of target motion such as vibrating, rotating, coning, and tumbling is illustrated in [13,14]; additionally, Kim et al. [15] demonstrated different human's motion aspects. All the above applications were carried out using conventional monostatic radar system architecture. Bistatic radar system has also been used in [10] for extracting the micro-Doppler signal. However, Forward scattering radar has many distinct advantages compared to monostatic and bistatic counterparts. These advantages can be summarized as [16,17]: (i) enhancement in target RCS; (ii) relatively simple hardware structure; (iii) high ability to detect stealth targets regardless to the target's shape or coating materials; and (iv) absence of target phase fluctuations that make coherent signal processing possible over the full visibility time of the target.

Despite the advantages of using the micro-Doppler in target classifications, no results have been published for studying the capability of using the FSR to detect the micro-Doppler, except our research group published paper [18]. Nevertheless, there is still a need for more studies, investigations and improvements on using the FSR for micro-motions detections. Therefore, the aim of this paper is to carry out detail analyses (theoretical and experiment) to prove the FSR capability for detecting diverse micro-motion scenarios such as swinging pendulum and human parts. In addition, the effect of speed and direction of swinging to the micro-Doppler signature as well as multi micro-Doppler detections are also investigated. The information gathered and results produced can be beneficial for remote monitoring such as human fall detection, human gait recognition, perimeter fencing, intelligent target recognition and biomedical applications.

This paper is organized as follows: Section 2 presents the mathematical analyses for the FSR micro-Doppler detection for a pendulum swinging on the baseline between Transmitter (Tx)–Receiver (Rx), followed by simulation illustrations of the swinging pendulum. The experimental investigations are presented in Section 3 which includes the micro-Doppler results for swinging pendulum and human parts. The conclusion and future works are given Section 4.

2. Mathematical and Simulation Analyses for Micro-Doppler in FSR System

2.1. Doppler Frequency Generated from One Pendulum Swinging on FSR Baseline with Fixed Pivot

The analysis begins with Doppler frequency generated from the pendulum swinging and crossing the center of the baseline. Figure 1 illustrates the geometry of the FSR system used to observe the swinging characteristics of a dynamic mechanical pendulum attached to a fixed pivot. The Tx and Rx antenna facing each other and the operational region of FSR is near to the Tx–Rx baseline (BL) [19]. The range between the transmitter and pendulum is given by R_{Tx-Pen} and R_{Pen-Rx} represents the range between the pendulum and receiver. γ_{Tx} and γ_{Rx} are the transmitter–pendulum and pendulum–receiver elevation angles, respectively; β is the bistatic angle; and θ is the swinging angle (angular displacement) of pendulum. A represents the maximum linear displacement when the pendulum is at the maximum angular displacement. The transmitter and receiver antennas are elevated at h_{min} , which also represents the height of the BL between the transmitter and receiver. h_{max} is the maximum height when the pendulum is at maximum displacement, and P is the pendulum's pivot point which is the center for the pendulum swing with coordinate (x',y',z') . The system coordinate (X,Y,Z) is centered at the middle point of the baseline.

In the proposed FSR system, the transmitter transmits a continuous wave signal, and the receiver receives a direct signal, S_d as well as the signal scattered, S_c by the pendulum. The total range of the signal scattered by the pendulum is the sum of the ranges from the transmitter to the pendulum R_{Tx-Pen} and from the pendulum to the receiver R_{Pen-Rx} . If the pendulum swings with a tangential velocity, V_r , the scattered signal phase, ϕ_c , in S_c changes with time and given by [17]:

$$\phi_c(t) = \frac{2\pi}{\lambda_c} (R_{Tx-Pen}(t) + R_{Pen-Rx}(t)) \quad (1)$$

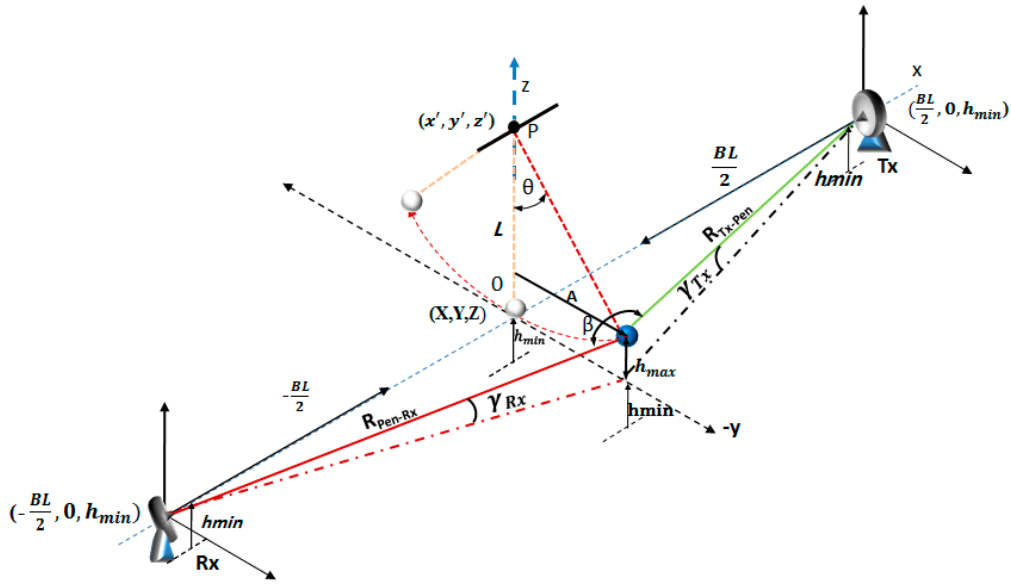


Figure 1. Forward Scatter Radar geometry to observe Doppler from the swinging pendulum crossing Transmitter (Tx)–Receiver(Rx) baseline.

The Doppler frequency f_d can be obtained by the time derivative of phase change of Equation (1) [19]:

$$f_d(t) = \frac{1}{\lambda_c} \left[\frac{d}{dt}(R_{Tx-Pen}(t)) + \frac{d}{dt}(R_{Pen-Rx}(t)) \right] \quad (2)$$

where the terms $\frac{d}{dt} R_{Tx-Pen}(t)$ and $\frac{d}{dt} R_{Pen-Rx}(t)$ represent the projections of the pendulum’s velocity vectors onto the line of sight between the radar transmitter–pendulum and pendulum–receiver, respectively; thus, in bistatic radar, the general expression of Doppler frequency is given by [19]:

$$f_d = \frac{1}{\lambda_c} \left[V_r \cos\left(\frac{\beta}{2} - \delta\right) + V_r \cos\left(\frac{\beta}{2} + \delta\right) \right] \quad (3)$$

$$f_d = \frac{2V_r}{\lambda_c} \cos\left(\frac{\beta}{2}\right) \cos\delta \quad (4)$$

where δ is the target aspect angle, which is the angle between the bisection line normal to the BL and the target direction of motion. In this paper, the ranges R_{Tx-Pen} and R_{Pen-Rx} are assumed to be equal, thus the aspect angle is $\delta = 0$. According to Figure 1, the pendulum is forward shifted by an initial angular displacement θ_0 . This is the initial swinging position of the pendulum at $t = 0$. The pendulum continues to swing from forward to backward and it crosses the BL in each trip. If the location of the transmitter and receiver are given by:

$$Tx = \left(\frac{BL}{2}, 0, h_{min} \right) \quad (5)$$

$$Rx = \left(-\frac{BL}{2}, 0, h_{min} \right) \quad (6)$$

thus, the initial coordinate of the pendulum mass, m_{pd} is:

$$m_{pd}(0) = (0, A, h_{min} + h_{max}) \quad (7)$$

The maximum linear displacement of pendulum, A , can be found by:

$$A = L \sin(\theta_0) \quad (8)$$

where L is the length of pendulum's cord. When the pendulum is positioned at the maximum angular displacement, then the maximum height h_{max} of the pendulum mass is given by:

$$h_{max} = L(1 - \cos(\theta_0)) \quad (9)$$

The initial range from Tx to the pendulum mass, $R_{0(Tx-Pen)}$ and from the pendulum mass to Rx, $R_{0(Pen-Rx)}$ are given by Equations (10) and (11), respectively:

$$R_{0(Tx-Pen)} = \sqrt{(X_{Tx} - x_{0(Pen)})^2 + (Y_{Tx} - y_{0(Pen)})^2 + (Z_{Tx} - z_{0(Pen)})^2} \quad (10)$$

$$R_{0(Pen-Rx)} = \sqrt{(x_{0(Pen)} - X_{Rx})^2 + (y_{0(Pen)} - Y_{Rx})^2 + (z_{0(Pen)} - Z_{Rx})^2} \quad (11)$$

When the pendulum starts to swing, the angular displacement θ changes with time, therefore, the instantaneous angular displacement can be expressed by [20]:

$$\theta(t) = \theta_0 \cos(\omega_0 t) \quad (12)$$

where ω_0 is the angular frequency given by $\omega_0 = \sqrt{\frac{g}{L}}$, and g is acceleration of gravity.

The instantaneous pendulum mass coordinates becomes:

$$m_{pd}(t) = (0, L \sin(\theta_0 \sin(\omega_0 t)), h_{min} + L(1 - \cos(\theta_0 \sin(\omega_0 t))) \quad (13)$$

then, the instantaneous ranges from the transmitter to the pendulum and pendulum to the receiver are given by:

$$R_{Tx-Pen}(t) = \sqrt{(X_{Tx} - x_{pen}(t))^2 + (Y_{Tx} - y_{pen}(t))^2 + (Z_{Tx} - z_{pen}(t))^2} \quad (14)$$

$$R_{Pen-Rx}(t) = \sqrt{(x_{pen}(t) - X_{Rx})^2 + (y_{pen}(t) - Y_{Rx})^2 + (z_{pen}(t) - Z_{Rx})^2} \quad (15)$$

the swinging pendulum Doppler frequency, fd_{pen} , is given by Equation (16):

$$fd_{pen}(t) = \frac{2 \times V_{Pen-Tang}(t)}{\lambda_c} \cos(\beta_{pen}(t)/2) \cos \delta_{pen} \quad (16)$$

$$\beta_{pen}(t) = \cos^{-1} \left(\frac{R_{Tx-pen}^2(t) + R_{pen-Rx}^2(t) - BL^2}{2 \times R_{Tx-pen}(t) \times R_{pen-Rx}(t)} \right) \quad (17)$$

$$V_{Pen-Tang}(t) = L \times \Omega(t) \quad (18)$$

where β_{pen} and $V_{Pen-Tang}$ are the bistatic angle and tangential velocity of pendulum, respectively. The pendulum angular velocity $\Omega(t)$ is the first derivative of the angular displacement $\theta(t)$ depicted by Equation (12). The pendulum angular velocity can be expressed by:

$$\Omega(t) = \frac{d\theta(t)}{dt} = -\theta_0 \omega_0 \sin \omega_0 t \quad (19)$$

Equations (12) and (19) show that the angular velocity of the pendulum, $\Omega(t)$ reaches maximum value when the pendulum is at the lowest point (equilibrium position), i.e., $\theta(t) = 0$ rad, and the angular velocity of pendulum is lowest when the pendulum is at the highest position, i.e., $\theta(t) = \theta_0$ rad.

The simulation for the above derivation is carried out for the swinging pendulum in the FSR system which is shown in Figure 1. A continuous wave with a frequency of 3 GHz is used as a transmitted signal for three different values of initial angular displacements $\theta_0 = 20^\circ$, 40° and 70° .

The BL length between the transmitter Tx and receiver Rx is 6 m. The length of pendulum string is 1 m and thus the maximum linear displacements travelled by the pendulum, A , are 0.34, 0.64, and 0.94 m for three values of initial angular displacement θ_0 . The effect of the additive noise, the multipath effect and the effect of clutter noise are neglected in this simulation.

As illustrated in Figure 1, the pendulum swings above the center line (Y-coordinate) between the transmitter and receiver. The equivalent signal (Doppler signal) at the receiving antenna is constructed due to the interference between the direct signal (transmitted carrier) from the transmitter and the scattered signal from the target. This Doppler signal suffers from phase and amplitude modulation caused by the interference of these two signals. The phase and amplitude modulated signal can be extracted by using an appropriate signal processing algorithm (self-mixing demodulation technique) [16,17,21]. Here, the output signal from the demodulation process is defined as a Doppler signature, which is a time domain signal with an amplitude of volt. The Doppler signature signal possesses information on the target's (or pendulum) motion characteristics [13]. The Doppler signature in time domain for a forward-shifted pendulum by 70° is illustrated in Figure 2a and it is compared with the instantaneous changing of coordinates in the pendulum position relative to the baseline, which is represented by the dashed line in Figure 2a. The pendulum swings along the center line with a maximum linear velocity of 3.59 m/s, while the pivot point is fixed at the location of $(0,0,(L + h_{\min}))$, relative to the system coordinates (X,Y,Z) . As shown in Figure 2a, the frequency of Doppler signature is high and its amplitude is low when the pendulum is moving away from the baseline, while the frequency reduces and the amplitude increases in two positions: the first is when the pendulum approaches to the baseline and the second is when the pendulum speed is approach to zero (Stopping). When the pendulum exactly crosses the baseline, the frequency and amplitude of Doppler signature are equal to zero. At the baseline the Doppler frequency equals zero because the bistatic angle β_{pen} equals 180° as depicted in Equation (4), and the amplitude becomes minimum or zero because the direct and scattered signals are equal and opposite each other in phase [18]. The BL crossing points are marked by circles. The red circle indicates the points when the pendulum crossed the BL while it moves backward, and the black circles indicate crossing points when the pendulum moves in forward. When the pendulum speed approaches to zero at the maximum position, then its Doppler frequency is approaching to zero too as depicted in Equation (4), which is clearly observed in Figure 2a. Despite the zero Doppler but the amplitude is high because in this case the frequency of the scattered signal is equal to the transmitted carrier frequency. After self-mixing demodulation and low-pass filtering, the output signal is just the DC component which is equal to $\left(\frac{A_c^2 + A_{sc}^2}{2}\right)$, where A_c is the maximum amplitude of the transmitted signal and A_{sc} is the maximum amplitude of the scattered signal. In our simulation the value of A_c and A_{sc} are normalized to 1V. The maximum displacement points where the pendulum is stopped are shown in Figure 2a, and they are marked by squares; the red squares designate the backward maximum displacement while the black square designates the forward maximum displacement.

According to the time domain Doppler signature shown in Figure 2a, Figure 2b illustrates the time–frequency signature of the swinging pendulum, the maximum angular displacement of the pendulum marked by a black square, and the point when the pendulum crossed the BL is marked by a black circle. It can be noted that the Doppler frequency for both cases approach zero. In the first case, when the pendulum reaches its maximum angular displacement $\theta(t) = \theta_0$, the pendulum will stop to change its direction. At that moment, the pendulum velocity will be zero (the angular velocity $\Omega(t) = 0$ rad/s). Therefore, the Doppler frequency generated from the pendulum will be zero ($fd_{pen}(t) = 0$) based on Equation (16). In the second case, when the pendulum crosses the baseline, the pendulum bistatic angle $\beta_{pen}(t) = 180^\circ$, then ($fd_{pen}(t) = 0$).

Figure 3a,b shows the influence of linear velocity of the pendulum on the Doppler frequency performance for different values of initial angular displacement $\theta_0 = 40^\circ$ and 20° , corresponding to the tangential velocities of 2.14 m/s and 1.087 m/s, respectively. It is clearly noted that the Doppler frequency increases as the pendulum tangential velocity is increased, where the maximum Doppler

frequency was around 25 Hz in Figure 2a, while the Doppler frequency decreases as the pendulum tangential velocity is decreased as shown in Figure 3a,b, the maximum Doppler frequency is around 13 Hz and 7 Hz, respectively.

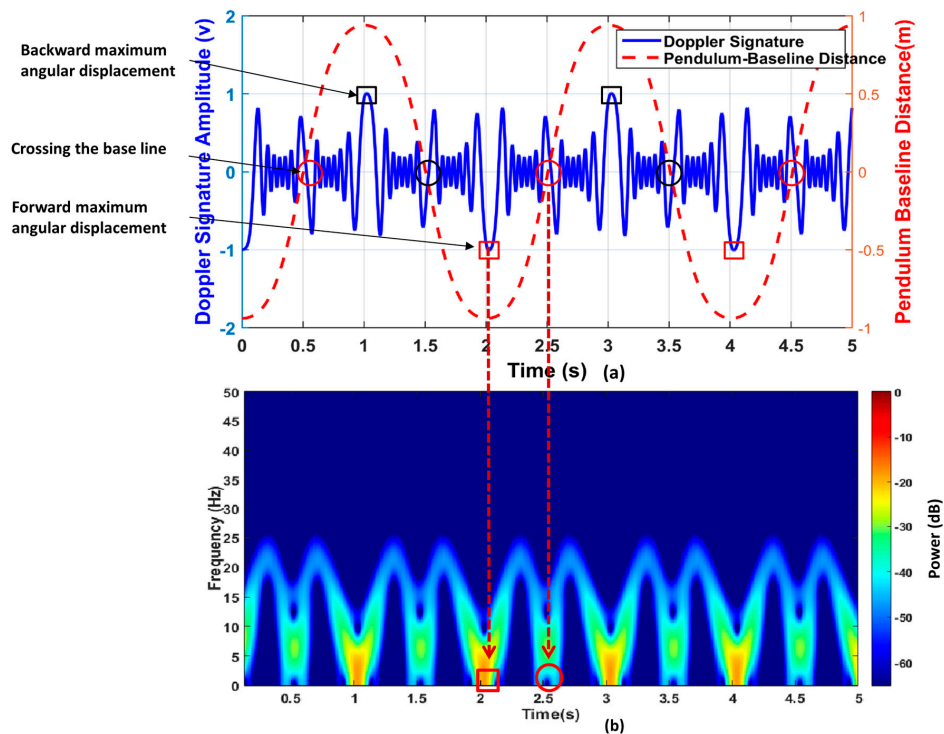


Figure 2. Simulation results of Doppler signature created from one pendulum swinging on the baseline with fixed pivot and initial angular displacement $\theta_0 = 70^\circ$: (a) time domain Doppler signature in comparison with the pendulum position relative to the baseline; and (b) spectrogram of Doppler signature.

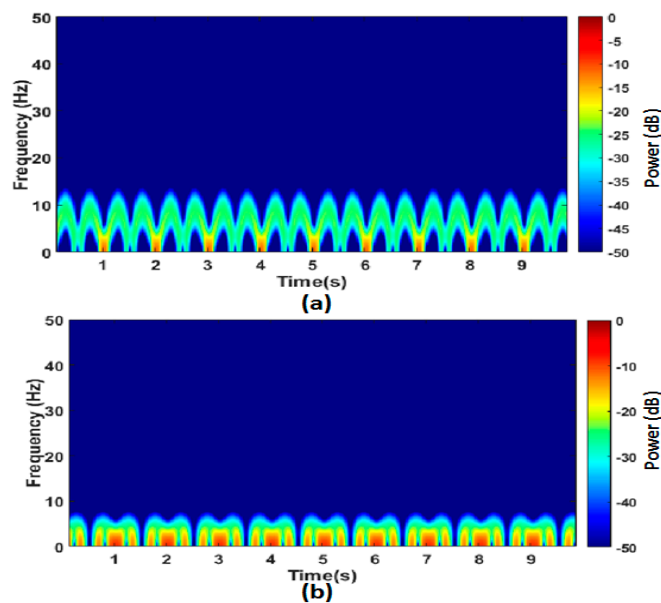


Figure 3. Spectrogram of the Doppler signature with one pendulum swinging on the BL with fixed pivot for initial angular displacement: (a) $\theta_0 = 40^\circ$; and (b) $\theta_0 = 20^\circ$.

2.2. Micro-Doppler Frequency Generated from One Swinging Pendulum with Moving Pivot in the FSR System

The simulation setup for this scenario is almost similar to the one for the previous scenario, but the total pendulum system coordinates are shifted along the Y-axis by distance of y_{max} as illustrated in Figure 4. The initial coordinate of the translational pendulum mass is:

$$m_{pd_t}(0) = (0, y_{max} - L \sin(\theta_0), h_{min} + L(1 - \cos(\theta_0))) \quad (20)$$

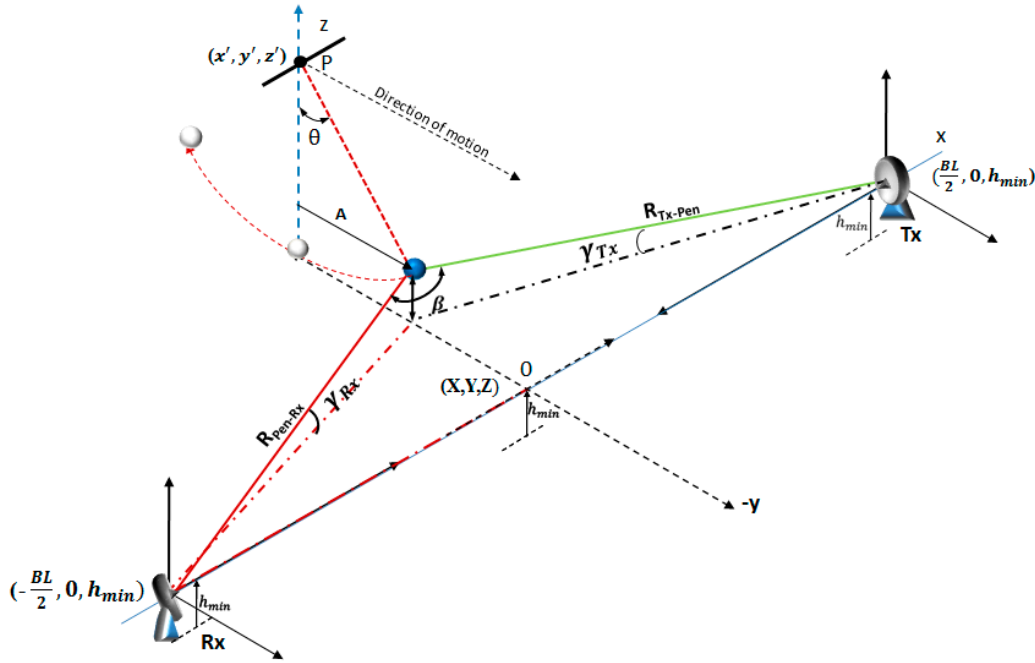


Figure 4. FSR geometry of forward-shifted pendulum with moving pivot point.

In this case, the pivot of pendulum p moves linearly from y_{max} to $-y_{max}$ along the Y-axis while the pendulum mass is swinging. Therefore, the coordinates of pendulum mass changes with time due to: (i) the vibration motion of pendulum; and (ii) the straight motion because of linear translation motion of its pivot point p . In Figure 4, the instantaneous translational coordinates of the pendulum mass are as follows:

$$m_{pd_t}(t) = (0, (y_{max} + (v_{pvt} \times t)) - L \sin(\theta_0 \sin(\omega_0 t)), h_{min} + L(1 - \cos(\theta_0 \sin(\omega_0 t))) \quad (21)$$

where v_{pvt} is the linear velocity of the pivot point. Then, the range of transmitter to pendulum mass (R_{Tx-Pen}), and the range of pendulum mass to receiver (R_{Pen-Rx}) can be expressed as:

$$R_{Tx-Pen}(t) = \sqrt{((BL/2) - 0)^2 + (0 - (y_{pen}(t)))^2 + (h_{min} - (z_{pen}(t)))^2} \quad (22)$$

$$R_{Pen-Rx}(t) = \sqrt{((-BL/2) - 0)^2 + (0 - (y_{pen}(t)))^2 + (h_{min} - (z_{pen}(t)))^2} \quad (23)$$

The bistatic angle can then be obtained by substituting Equations (22) and (23) into Equation (17). The pendulum Doppler frequency, which assembles with the two motions (the swinging motion and the translational motion), can be expressed as follow:

$$fd = \frac{2(V_{Pen-Tang} \pm V_{trans})}{\lambda_c} \cos \frac{\beta}{2} \cos \delta \quad (24)$$

where $V_{Pen-Tang}$ is the tangential velocity of the pendulum, which is previously given in (18), and V_{trans} is the translational motion due to the linear motion of the pendulum's assembly point (pivot point). The operator of \pm shows that the total velocity is the summation of $V_{Pen-Tang}$ and V_{trans} pendulum swings in a forward direction (i.e., with the same direction of the translation motion), while the total velocity is the difference between $V_{Pen-Tang}$ and V_{trans} for pendulum swings in backward direction (i.e., with the opposite direction of the translation motion).

For the scenario shown in Figure 4, the simulation is carried out for three different forward-shifted angles, $\theta_0 = 20^\circ$, 40° , and 70° which corresponds to the pendulum tangential velocities of 1.087 m/s, 2.14 m/s and 3.59 m/s, respectively. Figure 5 shows the time domain plot of the Doppler frequency signature of a moving pendulum assembly with a 20° shifted angle as shown in Figure 4. As shown in Figure 5, when the pendulum is released to start swinging from the initial forward-shifted position, it will move backward, thus the Doppler value will decrease (see Figure 6a) and after 1.15 s, the pendulum reaches the backward maximum position, and then it changes its direction of motion; therefore, the Doppler value will increase (see Figure 6a). As shown in Figure 5, the transition from the maximum forward position to maximum backward position takes 1.15 s, while the transition from maximum backward position to maximum forward position takes 1.98 s periodically. The forward maximum positions of the pendulum are marked by the black circles, and the backward maximum positions are marked by red circles in Figure 5. The first black circle includes the initial forward maximum position of the pendulum. As the pendulum approaches the baseline, the Doppler value approaches to zero, and the phase of Doppler frequency signature will change by 180° when the pendulum crosses the BL, as shown in Figure 5 inside the large red circle at the center of the figure.

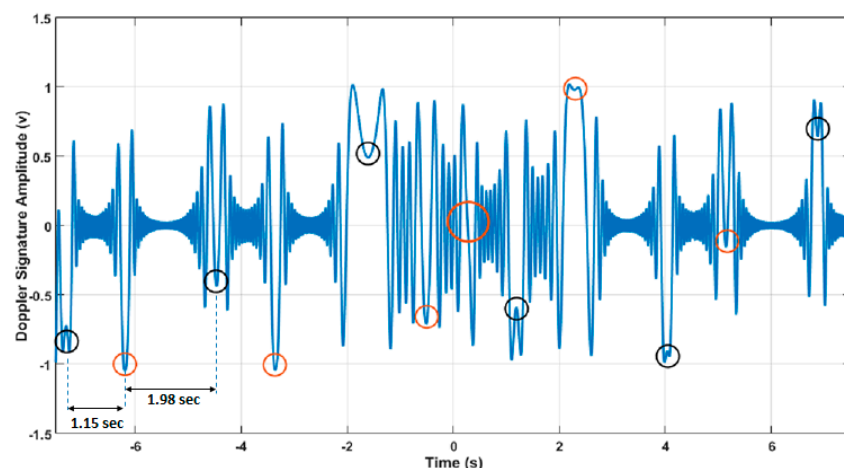


Figure 5. Simulation results of time domain Doppler signature created from one swinging forward-shifted pendulum with $\theta_0 = 40^\circ$.

The time–frequency distributions of the pendulum Doppler frequency signature with forward-shifted angles $\theta_0 = 20^\circ$, 40° and 70° are shown in Figure 6. As mentioned above, the value of pendulum Doppler frequency depends on the direction of the pendulum motion. When the pendulum starts to swing from the initial position (forward-shifted position), it moves backward, so, in this case, the value of Doppler frequency is a function of the subtraction of pendulum tangential velocity $V_{Pen-Tang}$ and the translational velocity of the whole pendulum assembly V_{trans} as expressed in Equation (24) with the minus sign. This behavior can be seen in Figure 6a during the time period from $t = 0$ s to $t = 1.15$ s. However, when the pendulum moves from backward to forward, the Doppler is higher than the backward motion, because its value is a function of the summation of the pendulum tangential velocity $V_{Pen-Tang}$ and the translational velocity of the whole pendulum assembly V_{trans} as given in Equation (24) with the plus (+) sign. This pattern can be seen from time $t = 1.15$ s to time $t = 3.13$ s in Figure 6a.

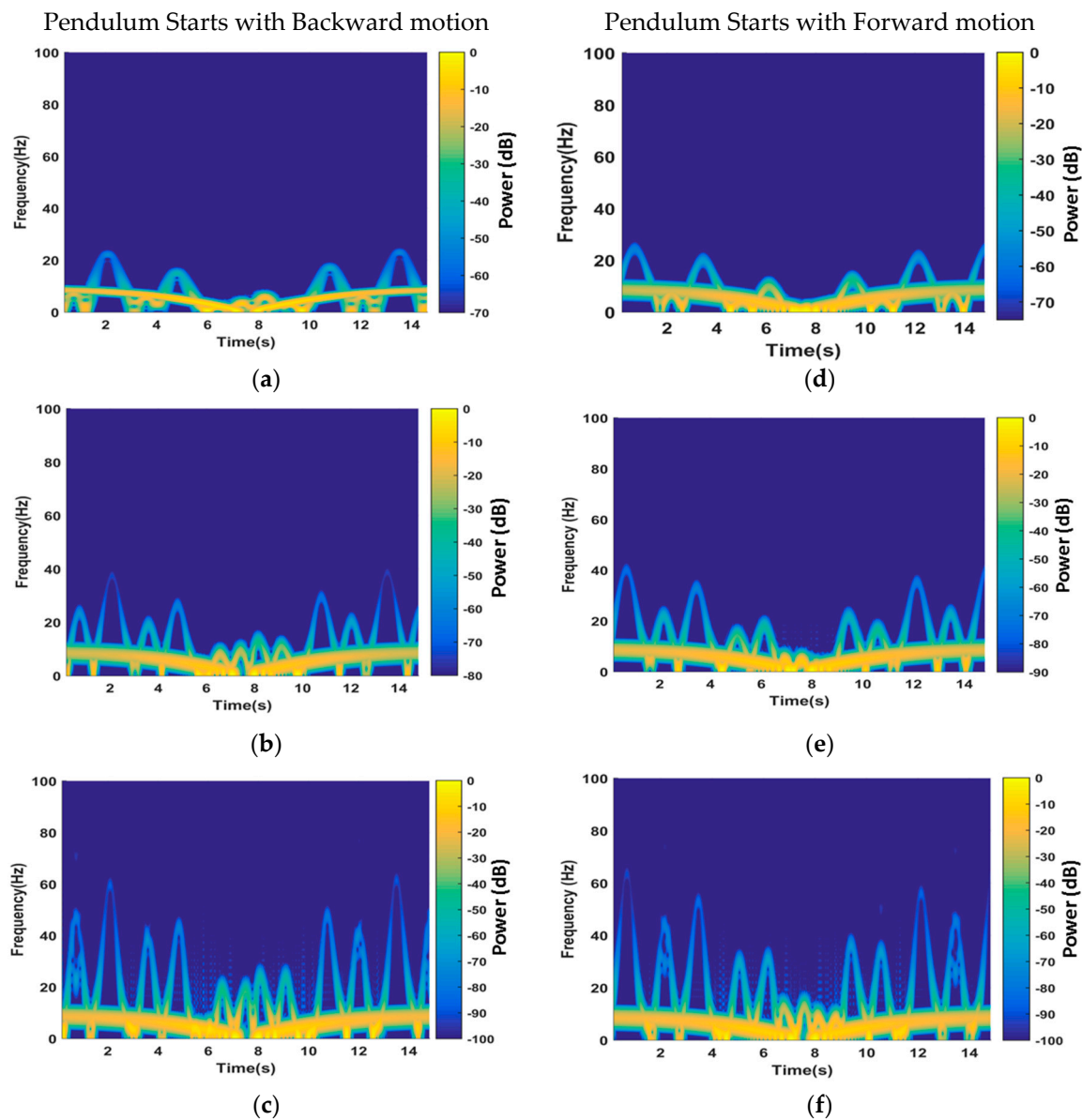


Figure 6. Simulation results for spectrogram of Doppler signature created from one swinging forward-shifted pendulum with: (a) $\theta_0 = 20^\circ$; (b) $\theta_0 = 40^\circ$; and (c) $\theta_0 = 70^\circ$; and Backward-shifted pendulum with: (d) $\theta_0 = 20^\circ$; (e) $\theta_0 = 40^\circ$; and (f) $\theta_0 = 70^\circ$.

The effect of increasing the tangential velocity of the pendulum is also noted in Figure 6a–c for different velocities (which is also different angles): 1.088 m/s, 2.14 m/s and 3.59 m/s, respectively. The maximum Doppler for the lowest pendulum tangential velocity is around 20 Hz Figure 6a, whereas it is around 40 Hz and 60 Hz for higher pendulum velocities Figure 6b,c respectively.

In order to verify the effect of forward and backward motions on the Doppler signatures, the same simulation setup is conducted but the pendulum mass is shifted to the backward position to start its swinging with a forward motion. Figure 6d–f illustrates the time–frequency signatures of oscillating pendulum with the initial angular displacements $\theta_0 = 20^\circ$, 40° and 70° , respectively. In the figures, it is clearly noticeable that the first cycle of the generated Doppler signature is higher than the second, as the first represents the Doppler generated pendulum while it is in a forward motion, whereas the second represents the Doppler when it is in a backward motion, which is matched with the abovementioned explanations depending on Equation (24).

2.3. Micro-Doppler Frequency Generated from Two Swinging Pendulums with Moving Pivot Point in the FSR System

In this scenario, micro-Doppler frequencies generated from two pendulums are considered. The pendulums swing simultaneously with one pendulum swing in forward direction, $+\theta_0$, while the other is backward-shifted, $-\theta_0$, within the FSR coordinate as illustrated in Figure 7. Other parameters are the same as in the previous subsections.

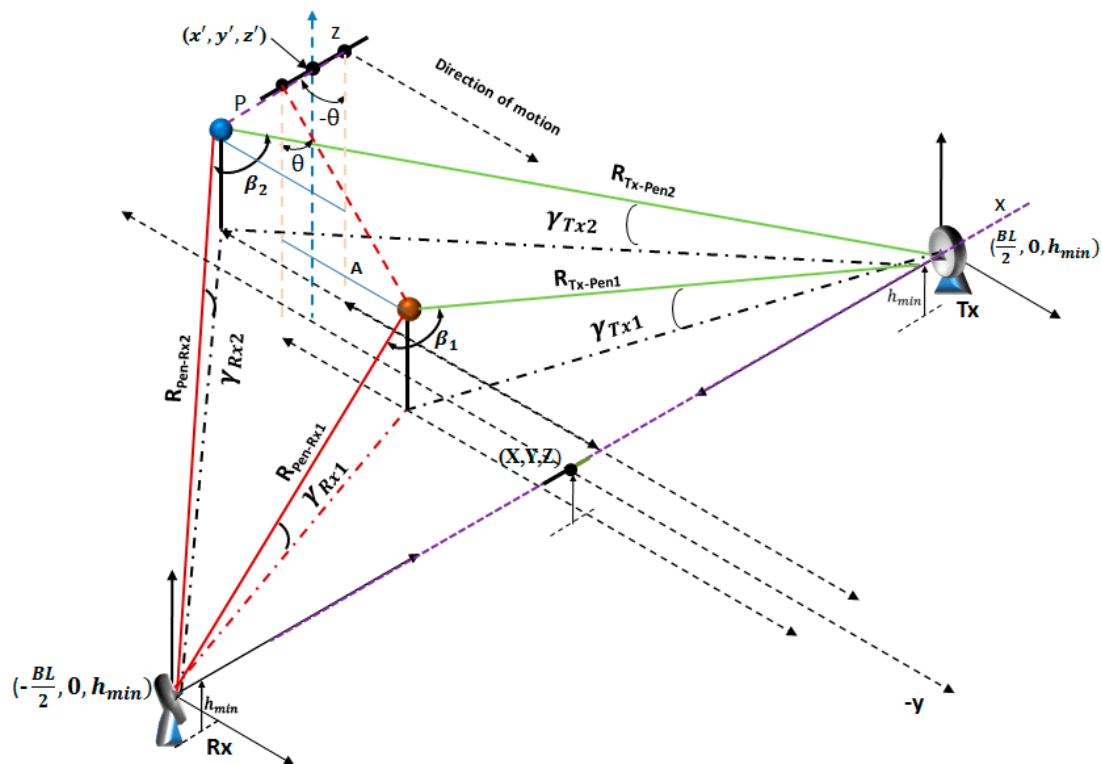


Figure 7. Two forward and backward-shifted pendulums oscillating in the FSR system.

Figure 8a shows the time–frequency signature for two oscillating pendulums at $\theta_0 = \pm 20^\circ$ for forward-shifted and backward-shifted Doppler frequency signature and the straight motion Doppler frequency signature respectively. The first higher half cycle represents the Doppler frequency signature for the backward-shifted pendulum and the first lower half cycle represents the Doppler signature for the forward-shifted pendulum. The backward-shifted pendulum starts with a high value of Doppler frequency; this is because the Doppler frequency is a function of the tangential velocity. In this case, the total linear velocity is the summation of the tangential velocity of the pendulum $V_{Pen-Tang}$ and the translational velocity V_{trans} as expressed in Equation (24) with the plus sign (+), while in the case of forward-shifted pendulum, the total velocity is the subtraction of the tangential velocity $V_{Pen-Tang}$ and the translational velocity V_{trans} as expressed in Equation (24) with the plus sign (+). Figure 8b,c illustrates the time–frequency signatures of forward and backward-shifted of two pendulums with angular displacements of $\theta_0 = 40^\circ$ and 40° , respectively. It is clearly shown that the Doppler frequency of the pendulum is higher when the pendulum starts to move from the backward position into forward, i.e., with the direction of translation motion (forward moving). Meanwhile, the Doppler frequency is lower when the pendulum starts to move from the forward position to backward, i.e., opposite to the translation motion direction (backward moving).

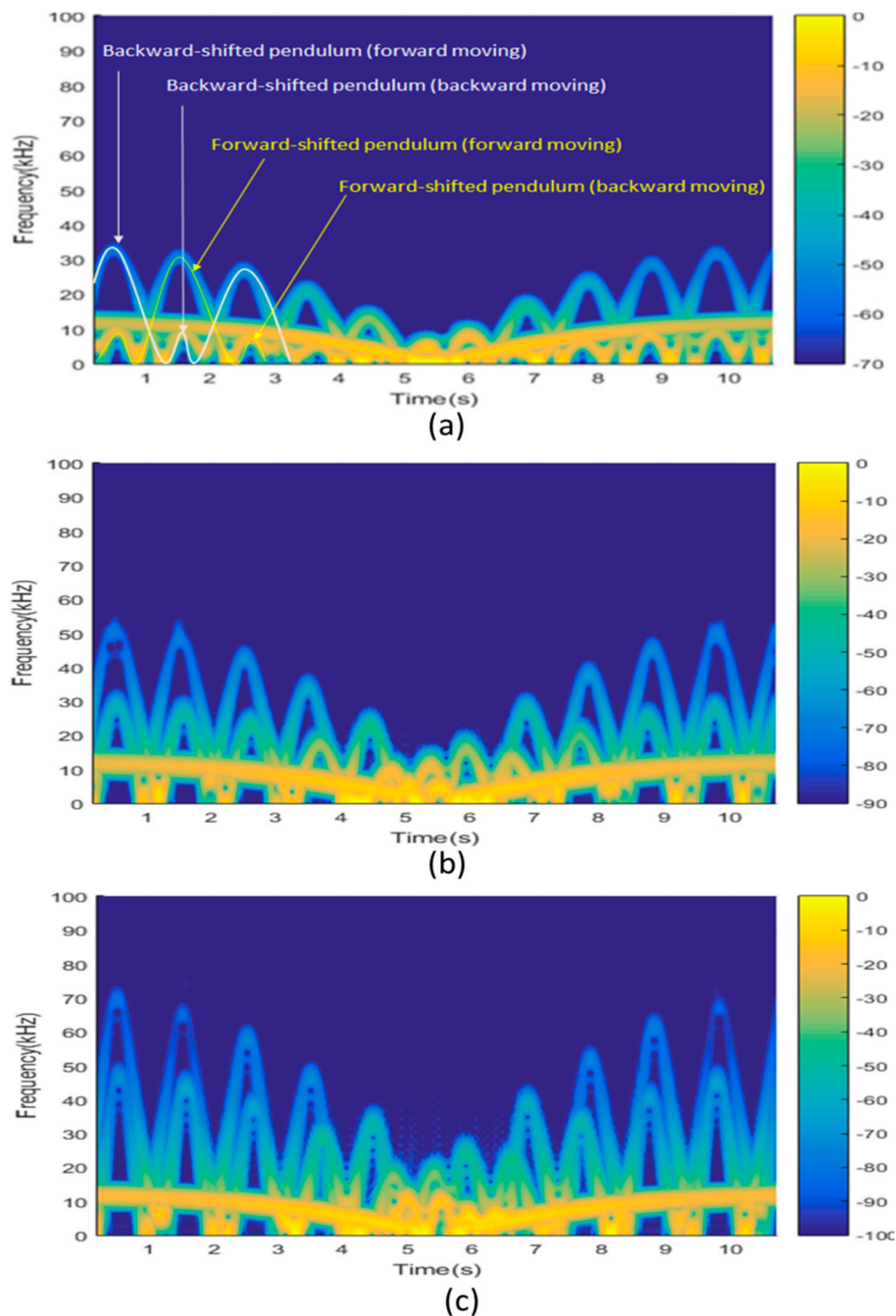


Figure 8. Simulation results for spectrogram of Doppler signature generated from two pendulums swing simultaneously in opposite direction with release angles, θ_0 at: (a) 20° ; (b) 40° ; and (c) 70° .

3. Experimental Results and Discussion for Micro-Doppler Detection in FSR

An experiment is carried out in a full scale anechoic chamber at the Malaysian National Space Agency (ANGKASA). The objectives of this experiment is: (i) to examine the performance of the FSR system in detecting and identifying micro-Doppler signatures generated from the micro-motions of different moving targets; and (ii) to understand the characteristics of micro-Doppler in the FSR system. The conducted experiment's setup is illustrated in Figure 9, and the experiment's real configuration inside the chamber is shown in Figure 10. The Tx and Rx are placed in FSR mode by facing each other and separated by a distance of 6 m (BL length). The trip of the moving object is 8 m, where the object crosses the BL perpendicularly. The height of both Tx and Rx is 0.85 m and the ground is partially

covered in absorbing material to illuminate the reflections from the ground. A 3 GHz CW signal with power of 10 dBm is generated from the signal generator and transmitted through a horn antenna. Unlike conventional radar systems, in this FSR system, only one receiving channel is required which is facing the Tx. This is due to the receiver that applies a self-mixing technique by the non-linear element (Diode); thus, it does not require any synchronization channel. When a moving target is entering the FS mode, two signals are scattered to the FS receiving antenna; a direct signal from the Tx, and a scattered signal from a moving target. Overall, the receiver circuit is designed to receive signals through a horn antenna which is connected directly with a Low Noise Amplifier (LNA) for amplifying the received signal. Subsequently, the amplified signal is passed through a non-linear diode detector to extract the Doppler signal and the detected signal passes through a low frequency circuit developed to filter out the high frequencies components by the Low Pass Filter (LPF) and amplify the low frequencies by two stages of amplifiers. Thereafter, the signal is saved on the PC through ADC for post-processing.

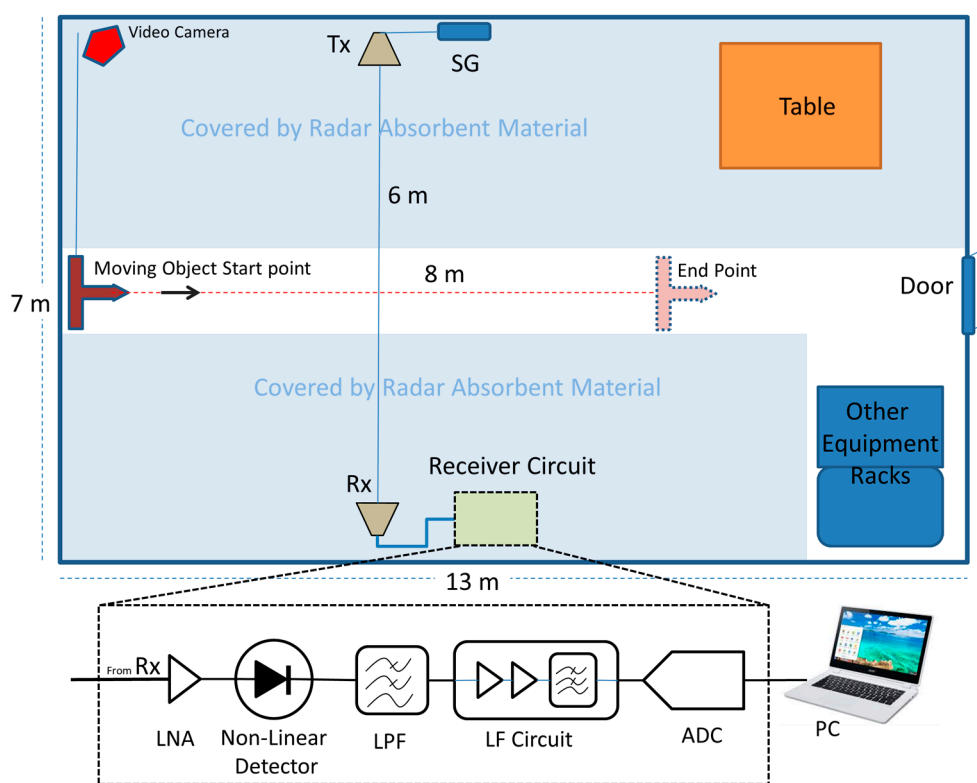


Figure 9. FSR Experimental setup and FSR circuit block diagram.

In this paper, four scenarios were conducted as listed in Table 1:

Table 1. Scenarios tested during the micro-Doppler experiment.

Scenario	Condition
A	One pendulum swings on the baseline. The pendulum is attached to the fixed gantry exactly at the top of the center of the baseline, and the pendulum mass crosses the BL with every swinging trip.
B	One pendulum attached to a stand placed on a moving trolley is used to investigate the effect of the pendulum’s swinging speed (pendulum tangential velocity) and swinging direction on Doppler signatures.
C	Two pendulums swing simultaneously at different directions.
D	A human stands on a moving trolley with swinging arms, then the human walks in a normal condition crossing the FSR baseline.

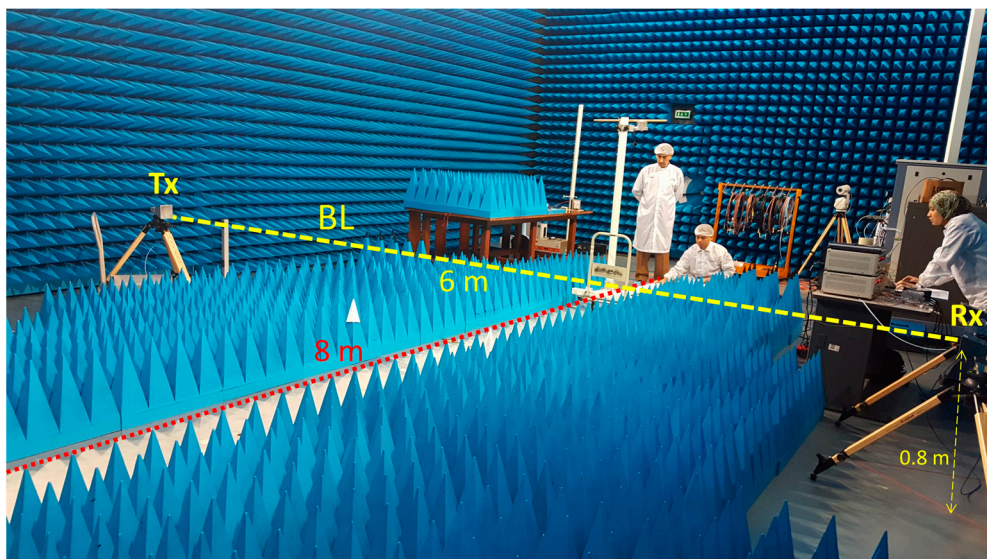


Figure 10. FSR experiment configuration inside the anechoic chamber.

3.1. Scenario A

In Scenario A, one pendulum is tied with a string and attached to a fixed stand at the other end. The pendulum swings cross perpendicularly to the BL as shown in Figure 11. Figure 12a shows the time domain for the Doppler signature detected for a recording time of 5.6 s. The experiment is conducted by placing the pendulum mass with an initial angle of displacement $\theta_0 = 40^\circ$, then it is released to start the swing in a forward motion. As we know, the pendulum tangential velocity increases until it reaches the maximum velocity at the equilibrium position where $\theta = 0^\circ$. In this scenario, the pendulum mass crosses the BL at this position, as in Figure 12a. Then, the pendulum angular velocity starts decreasing until it stops at the maximum displacement position, where the pendulum mass starts the reverse trip (backward). In Equation (17), the Doppler value generated from the swinging pendulum mainly depends on the tangential velocity of the pendulum and the pendulum bistatic angle β .

Figure 12b shows the time–frequency characteristics for the Doppler signature generated using a short-time Fourier transform (STFT) spectrogram on Matlab, with 3072 points Gaussian window that has a width of $\alpha = 3.5$, α which is proportional to the reciprocal of the standard deviation. The width of the window is inversely related to the value of α . A high pass Butterworth filter is used with a cutoff frequency of 1 Hz and order 1. The power in spectrogram is normalized to the maximum value, where the power is multiplied by a constant until the highest peak is equal to 1 (0 dB). It is clear from Figure 12a,b that the Doppler value starts from near zero and increases with the increase of the pendulum tangential velocity until the pendulum mass crosses the BL, $\beta = 180^\circ$, where the Doppler value drops to zero at point A, regardless of the pendulum's tangential velocity, which is the maximum at this position. After point A, the Doppler value increases again as β decreases, where the pendulum mass is going far from the BL. At the same time, the tangential velocity of the pendulum decreases until it stops at the maximum displacement position; therefore, the Doppler value is zero again at point B. The same scenario happens in a backward motion where the Doppler value is zero at point C and D when the pendulum crosses the BL and when it stops to change the motion direction, respectively. The spectrogram for the experimental results match with the simulation results shown in Figure 2b where the Doppler approaches to zero in two positions; the first position is when the pendulum mass crosses the BL (i.e., $\beta = 180^\circ$) and the second position is when the pendulum reaches the maximum displacement.

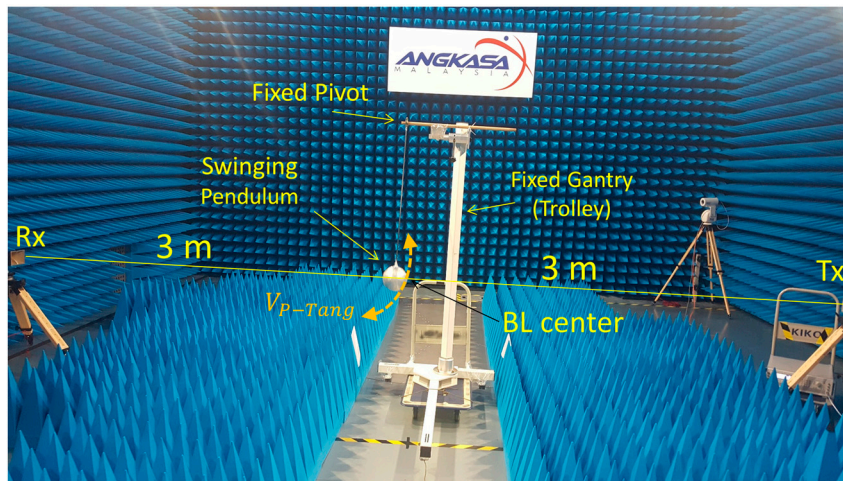


Figure 11. Scenario A configuration, one pendulum crossing the baseline.

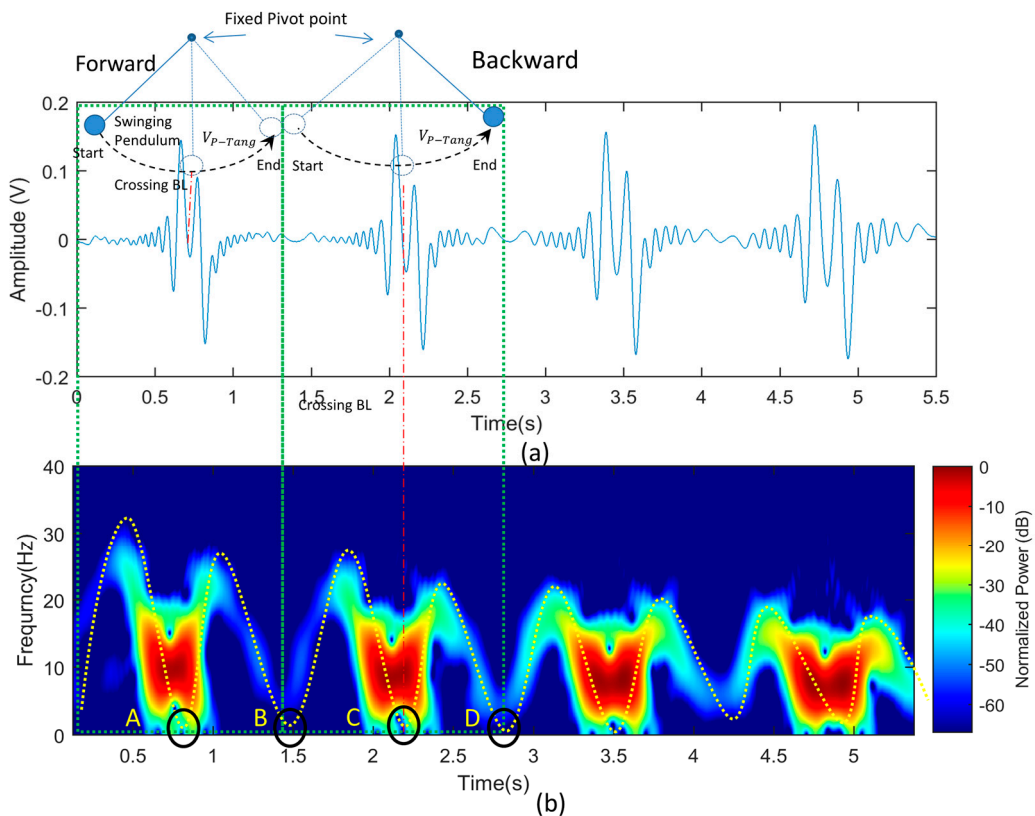


Figure 12. Scenario A, the pendulum swinging in the BL: (a) the time domain for Doppler signature generated from the swinging pendulum; and (b) the spectrogram of Doppler signature.

3.2. Scenario B

In Scenario B, a pendulum attached to a stand placed on a moving trolley is used. The trolley resembles the non-fluctuating object and the pendulum resembles the micro-motion of the object. The swinging of pendulum describes the micro-motion that generates frequency modulated carrier on the scattered signal and induces a micro-Doppler effect in addition to the Doppler frequency shift due to translation motion. In this testing, two signals (Doppler frequency shift) are received by the receiver, which comprises of the Doppler frequency due to the translation motion (moving trolley),

and micro-Doppler due to the micro-motion (swinging pendulum). The first stage of testing is to extract the Doppler frequency from only the moving trolley as a reference signal. The geometry of the conducted scenario is illustrated in Figure 13. The obtained result is shown in Figure 14, where the obtained Doppler from the moving trolley when it crosses the FSR BL appears as a straight line as the velocity of the trolley is maintained to be the same for the whole trip. It is noted that the Doppler value is between 5–10 Hz. When the trolley is far from the BL, and it is decreased as the bistatic angle β is increased until it becomes zero when the trolley crosses the BL (i.e., $\beta = 180^\circ$).

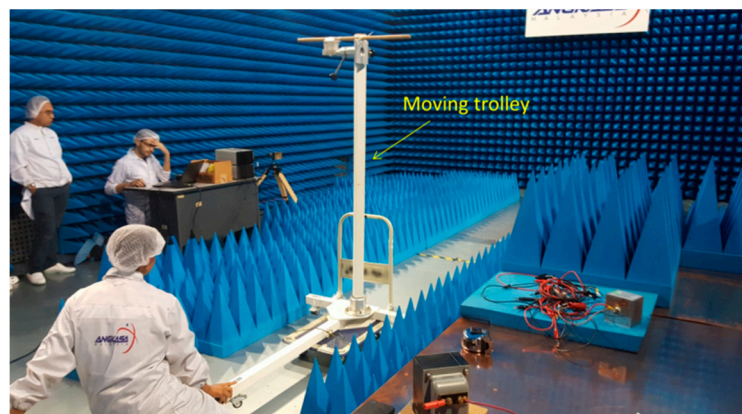


Figure 13. Moving trolley (without any micro motion) crossing the FSR baseline.

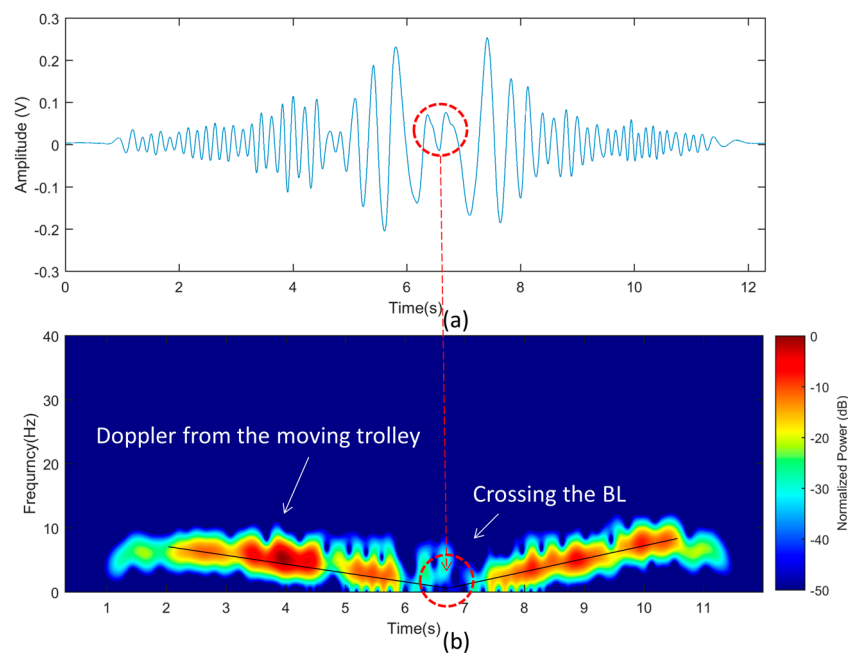


Figure 14. Experimental results of the moving trolley: (a) time domain Doppler signature; and (b) spectrogram.

In the second stage of this scenario, a pendulum is attached to the moving trolley to investigate the effect of the swinging pendulum when it starts moving in a forward motion, i.e., the pendulum is released to move with same direction of the trolley movement, as shown Figure 15. The obtained Doppler signature in the time domain and the spectrogram is shown in Figure 16. It is clearly illustrated in Figure 16b that the swinging pendulum adds a micro-Doppler with a sinusoidal shape, which matches the simulation results Figure 6. In this scenario, several swinging velocities are examined, as

the swinging speed is a function of the released angle (i.e., initial angular displacement, θ_0). The result shown in Figure 16 is for the swinging pendulum when the released angle $\theta_0 = 20^\circ$, where the maximum Doppler value is around 30 Hz, whereas the spectrograms shown in Figure 17a,b are for the pendulum released from angles $\theta_0 = 40^\circ$, and 70° which represent the medium and high speed, respectively. It is clearly shown that the Doppler signature for all speeds is a sinusoidal, and the maximum Doppler is increased as the pendulum speed is increased, where it is 30 Hz for the slow speed and around 45 Hz and 60 Hz for the medium and high speed, respectively.

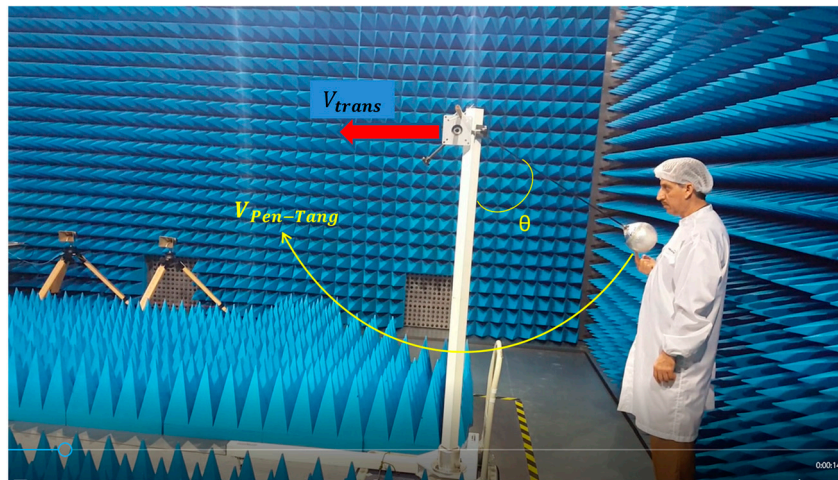


Figure 15. Experimental geometry for forward swinging pendulum.

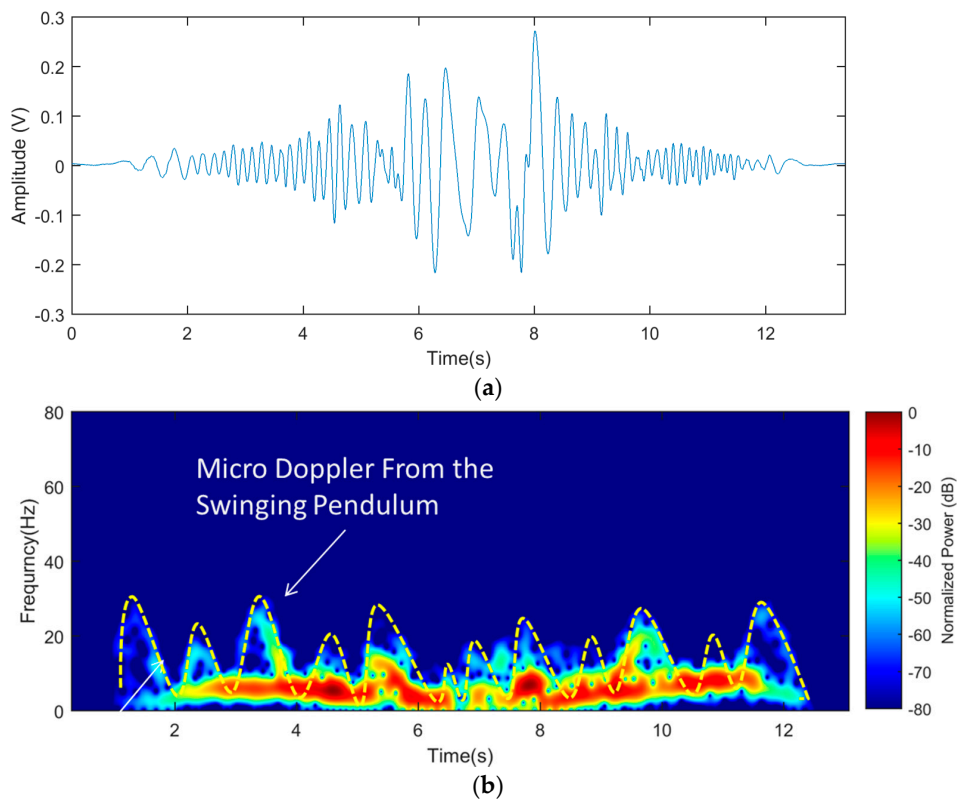


Figure 16. Pendulum swinging on the trolley in forward motion with a release angle, $\theta_0 = 20^\circ$: (a) time domain for Doppler signature; and (b) its spectrogram.

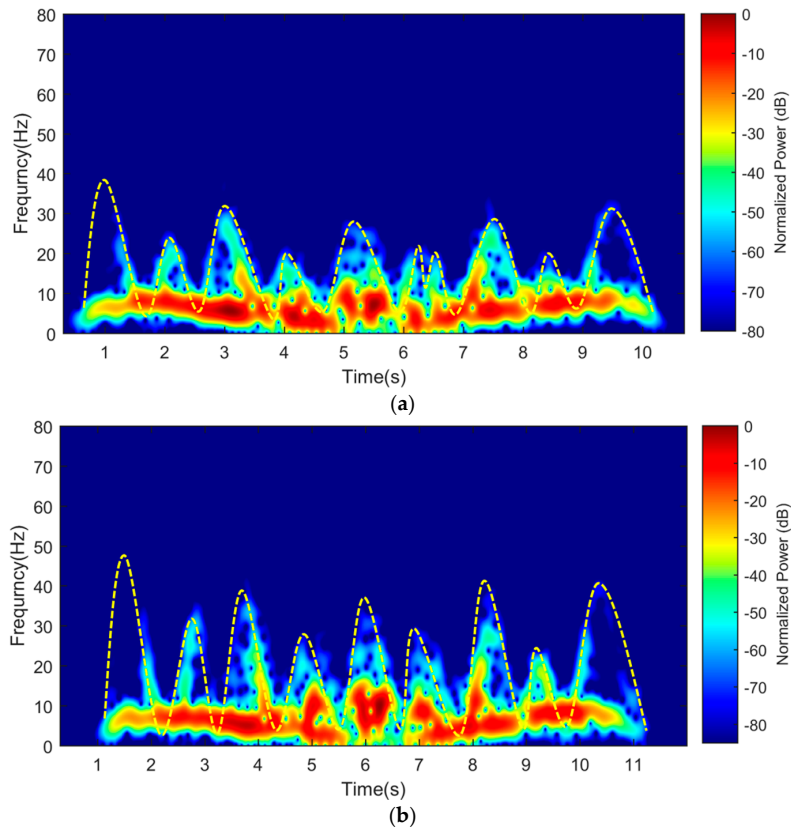


Figure 17. Spectrogram for one pendulum that starts moving in a forward motion when the release angles, θ_0 at: (a) 40° ; and (b) 70° .

Next is to conduct testing for the pendulum swings in a backward motion. The pendulum is placed in a forward shifted position to start its motion with a backward motion. The spectrogram for the Doppler signatures is shown in Figure 18 for the pendulum released at different release angle, θ_0 . In the figures, it is clearly shown that the Doppler for the first cycle for all θ_0 is lower than the second cycle. This is matched with the simulation results, where the total velocity in the first cycle is the subtraction of the pendulum tangential velocity $V_{pen-Tang}$ and the translational velocity V_{trans} of the whole pendulum assembly (Trolley velocity). It is a summation for the second cycle, as explained in Figure 19.

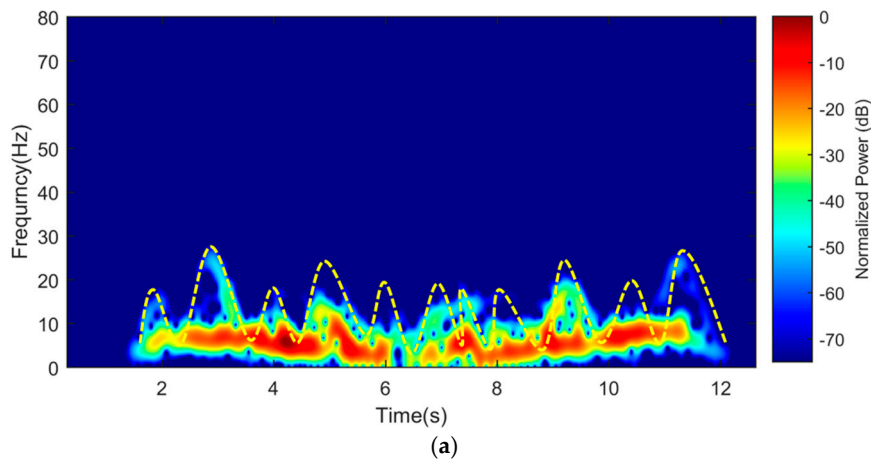


Figure 18. Cont

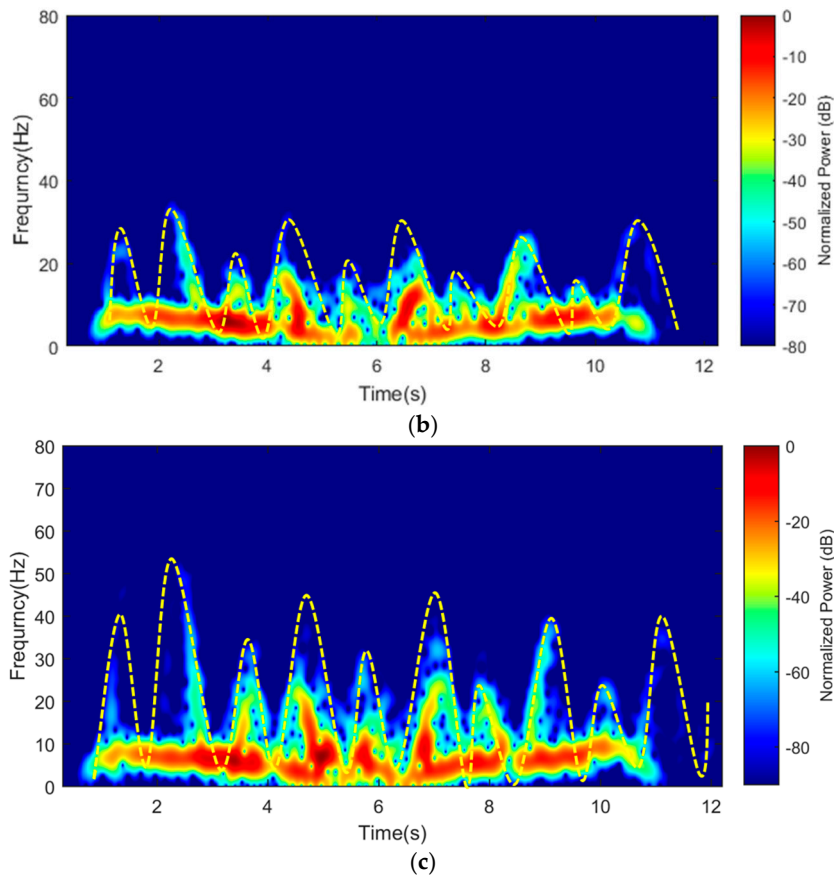


Figure 18. Spectrogram for one pendulum that starts moving in backward motion when the release angles, θ_0 at: (a) 20° ; (b) 40° ; and (c) 70° .

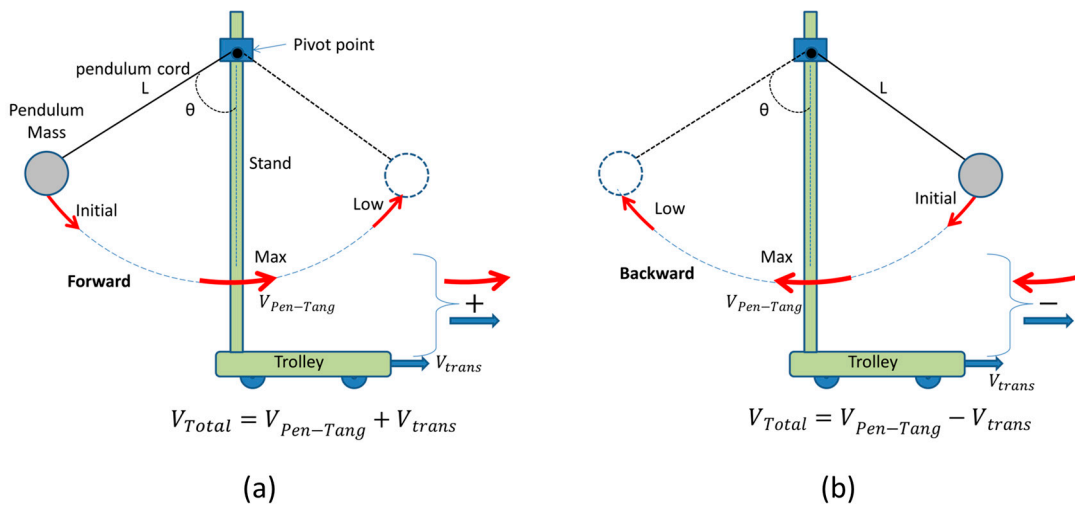


Figure 19. Pendulum swinging geometry with velocity analysis: (a) forward motion; and (b) backward motion.

3.3. Scenario C

Micro-Doppler signature scattered by two pendulums when they swing simultaneously at opposite direction to each other is analyzed in this scenario. The two pendulums are released when one of the pendulums is backward shifted while the other one is forward shifted with the same

release angle, as illustrated in Figure 20. Figure 21a–c shows the spectrogram plots of time–frequency signatures for two oscillating pendulums, when they forward and backward shifted with $\theta_0 = 20^\circ$, 40° and 70° , respectively.

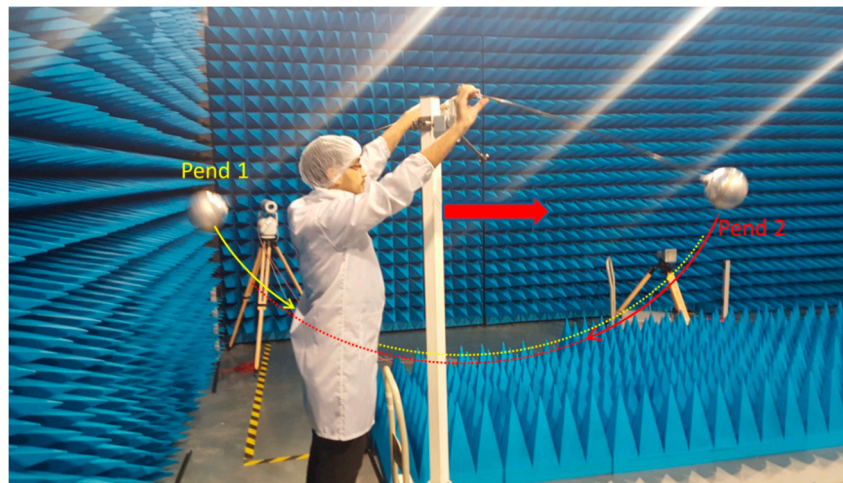


Figure 20. Two pendulums swinging simultaneously opposite to each other on a moving trolley.

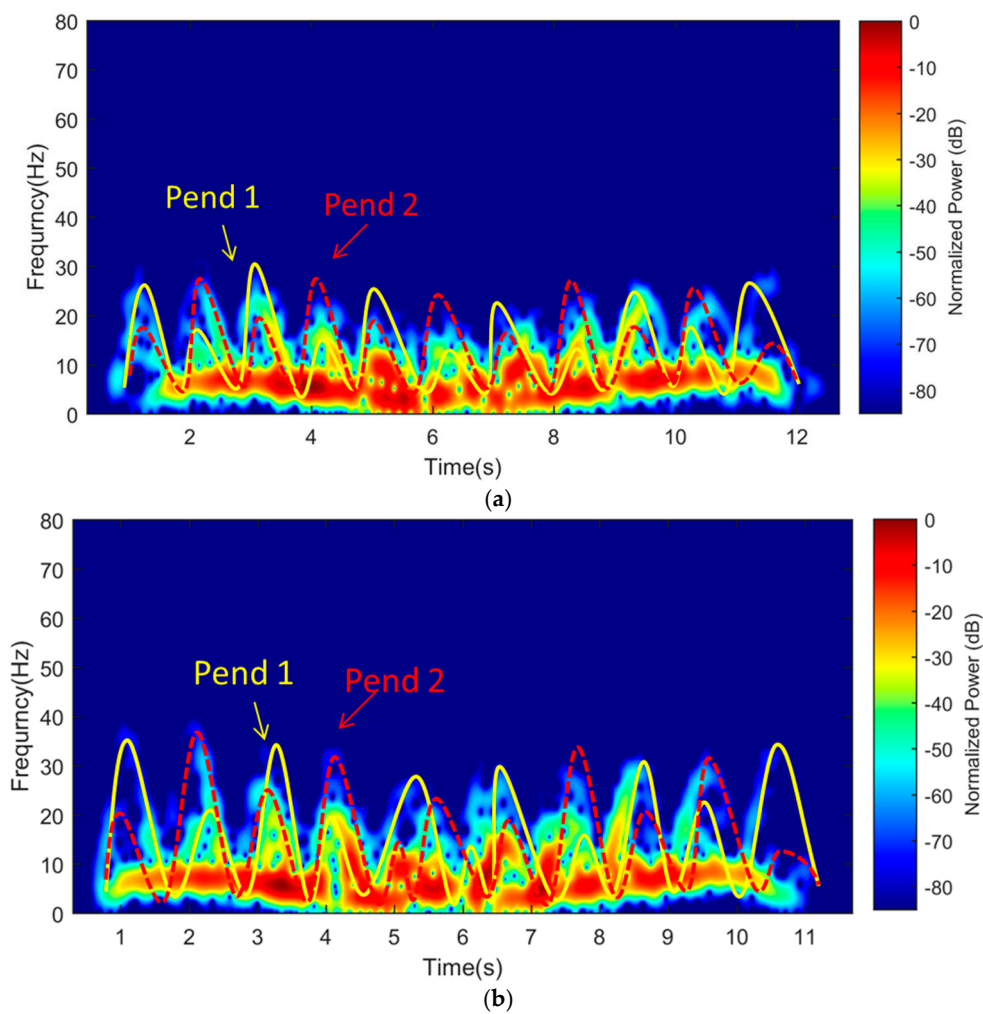


Figure 21. Cont.

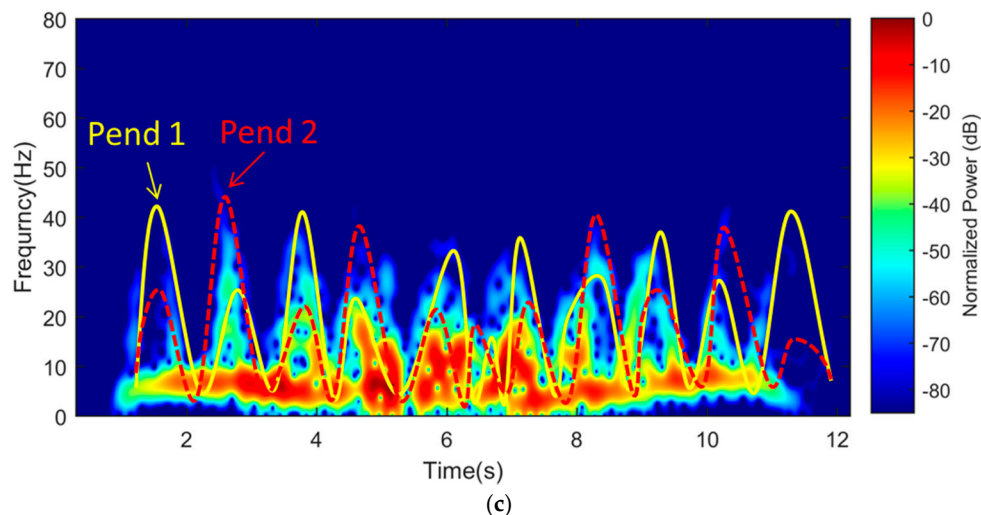


Figure 21. Spectrogram for two pendulums opposite to each other with release angles, θ_0 at: (a) 20° ; (b) 40° ; and (c) 70° .

It is clearly shown that the first higher half cycle represents the Doppler frequency signature for the backward-shifted pendulum and the first lower half cycle represents the Doppler frequency signature for the forward-shifted pendulum. Backward-shifted pendulum starts with a high value of Doppler frequency and this is because the Doppler frequency is a function of the linear velocity; in this case, the total linear velocity is the summation of the tangential velocity of the pendulum $V_{pen-Tang}$ and the translational velocity V_{trans} as expressed in Equation (24) with the plus sign (+). Meanwhile, in the case of forward-shifted pendulum, the total velocity is the subtraction of the tangential velocity $V_{pen-Tang}$ and the translational velocity V_{trans} as expressed in Equation (24) with the minus sign (-). Figure 21a,c illustrates the time–frequency signatures of forward and backward-shifted of two pendulums with the initial angular displacements $\theta_0 = 40^\circ$ and 70° . It is clearly shown that the Doppler frequency of the pendulum is high when the pendulum starts to move from the backward position with the direction of translation motion (forward moving), while the Doppler frequency is lower when the pendulum starts to move from the forward position that is opposite to the translation motion direction (backward moving).

3.4. Scenario D

The final scenario analyzes a more practical condition where human motion is used for testing. The experiment is started by having a human body and the swinging parts come from the hand only, while the human stands on a moving trolley. The objective of this scenario is to investigate the FSR system's capability to extract the micro-Doppler generated from the human's swinging hands. The spectrogram for the Doppler signature is illustrated in Figure 22. The micro-Doppler signature frequency generated from the oscillating hand appears as a sinusoidal, which is the same behavior of the swinging pendulum. However, the high frequency component, which represents the maximum velocity of the oscillating hand, disappeared (Figure 22 (position (b))). Based on the pendulum model analysis, the angular velocity of the pendulum reaches the maximum when the pendulum is at the lowest point (equilibrium position) of the swinging angle $\theta(t) = 0^\circ$. In the hand situation, this is achieved when the hand vector position is parallel to the body, which hides the hand from the receiver; therefore, the scattered signal is blocked. Consequently, the FSR receiver cannot detect this part of the signal. For further investigations, another experiment for the man swinging both hands is conducted and the obtained micro-Doppler is illustrated in the spectrogram in Figure 23. Two sinusoidal Doppler signatures with different cycles appear due to the swinging two hands. It is clear that the high Doppler frequency components also disappeared due to the same abovementioned reason.

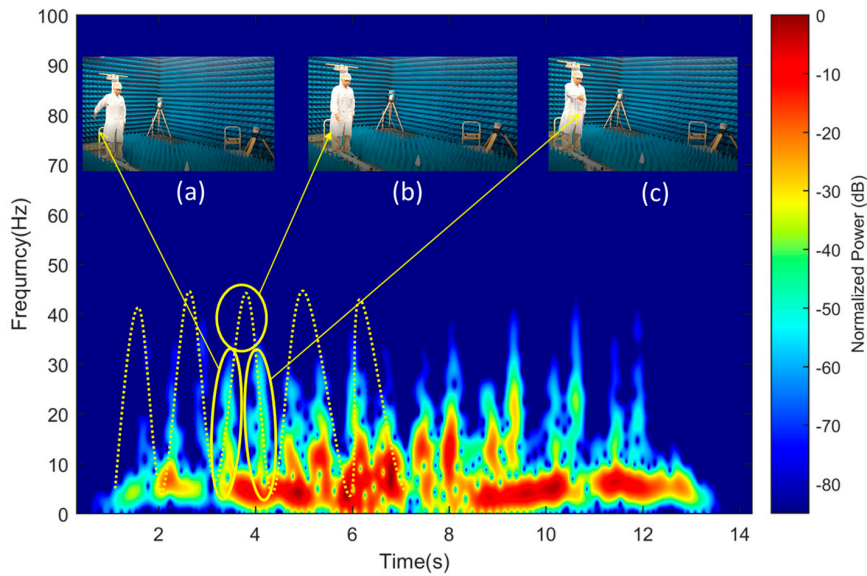


Figure 22. Spectrogram of Doppler signature for man standing on a moving trolley with one hand swinging.

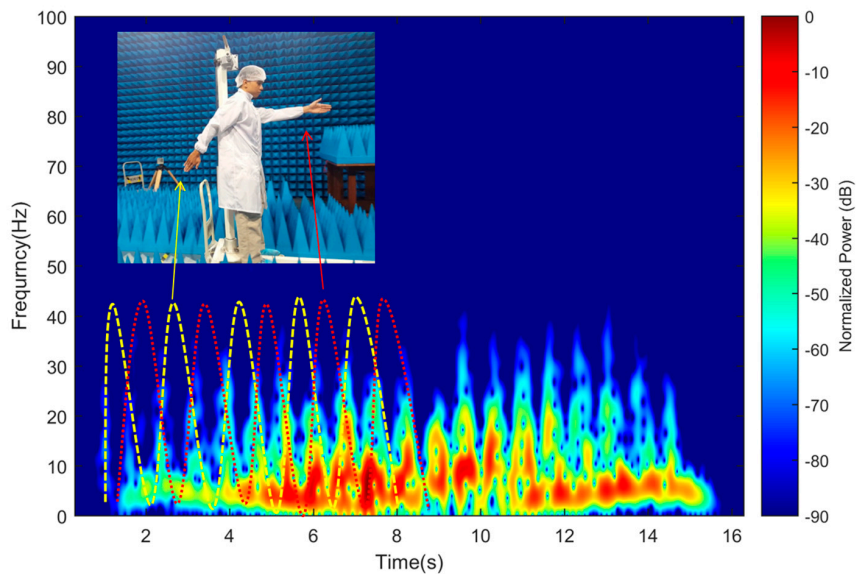


Figure 23. Spectrogram of Doppler signature for man standing on a moving trolley with two hands swinging.

For further investigation, an experiment is conducted on a normal human walking condition to examine the micro-Doppler for all human moving parts. Therefore, a man walking at a normal condition crosses the BL perpendicularly. The spectrogram for the Doppler signature generated from the walking micro-motions is illustrated in Figure 24. The figure shows the micro-Doppler produced from the hand and leg movements, where the micro-Doppler generated from the hands movements appear as strong peaks. However, the Doppler from the legs is not so clear due to blocking by the absorber. Nevertheless, the results obtained from this scenario give a good indicator that the FSR system has the capability to detect human movements. However, more classification techniques may be applied to analyze their behavior to be applied in several potential applications, such as recognition of individuals based on their walking gait and characterizing the elderly gait patterns with walking aids, which may allow the early detection of their fall events.

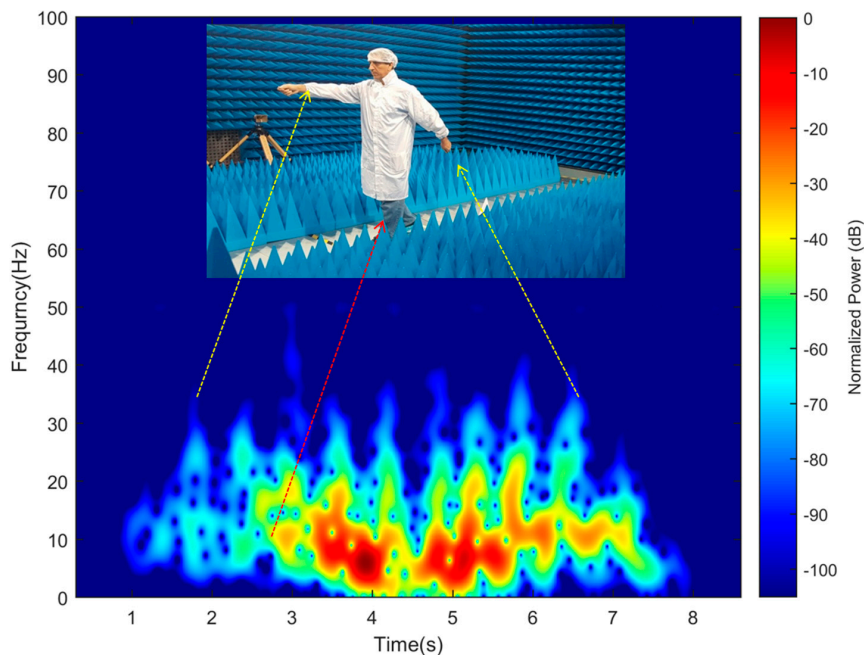


Figure 24. Spectrogram of Doppler signature for man normally walking and swinging two hands.

4. Conclusions

In this paper, the potential of the FSR system to extract micro-Doppler produced from the micro motion of pendulum and moving parts of the human body is studied and discussed. The analysis is supported by mathematical derivation, simulation and experimental result. The micro-Doppler frequency is clearly shown in the joint time–frequency representation. Few important observations from the time domain signal as well as spectrograms of the swinging pendulum can be listed: (i) the FSR can differentiate swinging direction based on the phase change and amplitude of the received signal; (ii) baseline crossing time can be predicted; and (iii) the micro-Doppler component can be easily extracted from the main Doppler. In addition, the experimental exploration on the possibility of FSR to detect micro-motion of human arms and legs is conducted. The system is capable to see the micro-Doppler from those human parts especially arms. However, it might have a situation where the Doppler information is poor, and this is mainly due to the hands hidden by the main body. This condition could be resolved by applying a multi-static system, the Single Input Multiple Output (SIMO) or Multiple Input Multiple Output (MIMO) approach, which allows for detecting the micro-motion targets from different viewing angles. The combination between the inherent advantages of FSR and with the ability to discriminate micro-Doppler enhance the FSR system prospect for many remote sensing and monitoring applications. Despite the positive results that have been obtained, it should be pointed out that there is still a need for further studies and improvements. A future study could give more attention on the system’s capability for detecting the micro-motion for different practical scenarios, e.g., human running, old man with aid tools, crawling man, and armed soldiers. In addition, more advanced signal processing algorithms could be applied to improve detection accuracy as well as target recognition.

Acknowledgments: The authors would like to express deep appreciation to the Malaysian National Space Agency (ANGKASA) for allowing the experiment to be conducted in their facilities, especially in the anechoic chamber.

Author Contributions: Raja Syamsul Azmir Raja Abdullah, Ali Alnaeb and Asem Salah designed the FSR prototype and signal processing scheme, analyzed the results, and performed the theoretical analysis and simulation. Nur Emileen Abdul Rashid, Aduwati Sali and Idnin Pasya analyzed the results and supported the manuscript preparation.

Conflicts of Interest: The authors declare no conflict of interest.

References

- Hiatt, R.; Siegel, K.; Weil, H. Forward scattering by coated objects illuminated by short wavelength radar. *Proc. IRE* **1960**, *48*, 1630–1635. [[CrossRef](#)]
- Raja Abdullah, R.S.A.; Rasid, M.F.A.; Mohamed, M.K. Improvement in detection with forward scattering radar. *Sci. China Inf. Sci.* **2011**, *54*, 2660–2672. [[CrossRef](#)]
- Abdullah, R.R.; Salah, A.A.; Aziz, N.A.; Rasid, N.A. Vehicle recognition analysis in LTE based forward scattering radar. *IEEE Radar Conf.* **2016**, *2016*, 1–5.
- Rashid, N.; Antoniou, M.; Jancovic, P.; Sizov, V.; Abdullah, R.; Cherniakov, M. Automatic target classification in a low frequency FSR network. In Proceedings of the 2008 European Radar Conference, Amsterdam, The Netherlands, 30–31 October 2008; pp. 68–71.
- Cherniakov, M.; Abdullah, R.R.; Jančovič, P.; Salous, M.; Chapursky, V. Automatic ground target classification using forward scattering radar. *IEE Proc. Radar Sonar Navig.* **2006**, *153*, 427–437. [[CrossRef](#)]
- Kabakchiev, H.; Behar, V.; Garvanov, I.; Kabakchieva, D.; Daniel, L.; Kabakchiev, K.; Gashinova, M.; Cherniakov, M. Experimental verification of maritime target parameter evaluation in forward scatter maritime radar. *IET Radar Sonar Navig.* **2015**, *9*, 355–363. [[CrossRef](#)]
- Salah, M.; Rasid, M.; Abdullah, R.R.; Cherniakov, M. Speed estimation in forward scattering radar by using standard deviation method. *Mod. Appl. Sci.* **2009**, *3*, 16. [[CrossRef](#)]
- Raja Abdullah, R.S.A.; Mohd Ali, A.; Rasid, M.F.A.; Abdul Rashid, N.E.; Ahmad Salah, A.; Munawar, A. Joint Time-Frequency Signal Processing Scheme in Forward Scattering Radar with a Rotational Transmitter. *Remote Sens.* **2016**, *8*, 1028. [[CrossRef](#)]
- Suberviola, I.; Mayordomo, I.; Mendizabal, J. Experimental results of air target detection with a GPS forward-scattering radar. *IEEE Geosci. Remote Sens. Lett.* **2012**, *9*, 47–51. [[CrossRef](#)]
- Clemente, C.; Soraghan, J.J. Vibrating target micro-Doppler signature in bistatic SAR with a fixed receiver. *IEEE Trans. Geosci. Remote Sens.* **2012**, *50*, 3219–3227. [[CrossRef](#)]
- Smith, G.; Woodbridge, K.; Baker, C.; Griffiths, H. Multistatic micro-Doppler radar signatures of personnel targets. *IET Signal Proc.* **2010**, *4*, 224–233. [[CrossRef](#)]
- Xu, Z.; Tu, J.; Li, J.; Pi, Y. Research on micro-feature extraction algorithm of target based on terahertz radar. *EURASIP J. Wirel. Commun. Netw.* **2013**, *2013*, 77. [[CrossRef](#)]
- Chen, V.C.; Li, F.; Ho, S.-S.; Wechsler, H. Micro-Doppler effect in radar: phenomenon, model, and simulation study. *IEEE Trans. Aerosp. Electron. Syst.* **2006**, *42*, 2–21. [[CrossRef](#)]
- Yang, Y.; Lei, J.; Zhang, W.; Lu, C. Target classification and pattern recognition using micro-Doppler radar signatures. In Proceedings of the Seventh ACIS International Conference on Software Engineering, Artificial Intelligence, Networking, and Parallel/Distributed Computing (SNPD'06), Las Vegas, NV, USA, 19–20 June 2006; pp. 213–217.
- Kim, Y.; Ling, H. Human activity classification based on micro-Doppler signatures using a support vector machine. *IEEE Trans. Geosci. Remote Sens.* **2009**, *47*, 1328–1337.
- Gashinova, M.; Daniel, L.; Hoare, E.; Sizov, V.; Kabakchiev, K.; Cherniakov, M. Signal characterisation and processing in the forward scatter mode of bistatic passive coherent location systems. *EURASIP J. Adv. Signal Proc.* **2013**, *2013*, 36. [[CrossRef](#)]
- Hu, C.; Sizov, V.; Antoniou, M.; Gashinova, M.; Cherniakov, M. Optimal signal processing in ground-based forward scatter micro radars. *IEEE Trans. Aerosp. Electron. Syst.* **2012**, *48*, 3006–3026. [[CrossRef](#)]
- Abdullah, R.R.; Salah, A.; Alnaeb, A.; Sali, A.; Rashid, N.A.; Ibrahim, I. Micro-Doppler detection in forward scattering radar: theoretical analysis and experiment. *Electron. Lett.* **2017**, *53*, 426–428. [[CrossRef](#)]
- Willis, N.J. *Bistatic Radar*, 2nd ed.; SciTech Publishing: Raleigh, NC, USA, 2005.
- Chen, V.C. *The Micro-Doppler Effect in Radar*; Artech House: London, UK, 2011.
- Sizov, V.; Cherniakov, M.; Antoniou, M. Forward scattering radar power budget analysis for ground targets. *IET Radar Sonar Navig.* **2007**, *1*, 437–446. [[CrossRef](#)]

